THE ASTROPHYSICAL JOURNAL, 329:241–252, 1988 June 1

THE EFFECTS OF PULSATION-EXTENDED ATMOSPHERES ON THE APPARENT DIAMETERS OF MIRA VARIABLES

T. E. BEACH, L. A. WILLSON, AND G. H. BOWEN
Astronomy Program, Department of Physics, Iowa State University
Received 1987 May 18; accepted 1987 November 18

ABSTRACT

Dynamic models of Mira atmospheres were analyzed to determine the limb darkening/brightening functions for a range of phases. The angular diameters that would be derived from lunar occultation observations of Mira variables with these limb functions were calculated. The results show that the usual procedure of fitting occultation observations assuming a uniform brightness disk and then correcting the resulting diameter for limb darkening can give erroneous results, and, in some cases, the "correction" can be a change in the wrong direction. Dynamic atmosphere effects cause Mira variables to appear larger and cooler than they actually are. The results presented here also have bearing on speckle interferometric measurements of Mira diameters where an assumed limb function must be used.

Subject headings: occultations — stars: atmospheres — stars: long-period variables — stars: pulsation

I. INTRODUCTION

Obtaining accurate angular diameters for Mira variables is vital for the determination of the effective temperature scale (Ridgway *et al.* 1980) and mode of pulsation (Willson 1982) for these stars. Measuring, or even defining, a diameter for a Mira variable has inherent difficulties. The diameter measured at different wavelengths can vary by more than a factor of 2, especially when observing in narrow bands near the absorption frequencies of molecules such as TiO (Labeyrie *et al.* 1977).

The extended nature of Mira atmospheres affects the diameter measured at any wavelength. The radius of the photosphere for a given wavelength is defined for models as the radius at which $\tau = \frac{2}{3}$ when integrating $d\tau = \kappa\rho\, dx$ inward along a line of sight toward the center of the star. When observing a stellar disk, however, the limb of the star will appear to be on the line of sight along which $\tau = \frac{2}{3}$ occurs at the tangent point. For an extended atmosphere, this line of sight will have an impact parameter which can be appreciably greater than the photospheric radius defined above, causing the star to appear larger than it actually is, as shown in Figure 1.

Mira atmospheres exhibit shocks which also can have a large effect on the limb darkening/brightening (limb function) of the star. In some regions of the spectrum, notably near the visual region, where postshock cooling radiation primarily occurs, most of the luminosity of the Mira variable comes from the shocks. Measurements of the diameter at these frequencies during phases when the shocks are strong will result in a diameter representative of the shock front and not the photosphere. This important effect is only apparent when using dynamic models for the atmosphere. Static model atmospheres, even with complete treatments of radiative transfer, are not valid in these cases. Apparent diameter enhancement due to shock emission is small in the infrared region where most lunar occultation studies are currently carried out.

II. LIMB FUNCTIONS AND OBSERVED ANGULAR DIAMETERS

The two primary methods of directly measuring stellar angular diameters, speckle interferometry and lunar occultations of stars, both depend upon assuming a limb function for the star in order to derive angular diameters from the observational data. In the case of lunar occultation observations, the Fresnel interference pattern that results as the Moon passes between the observer and the star is recorded. The shape of this light trace depends on the angular diameter and limb function of the star. The angular diameter is determined by comparing the data to a set of theoretical traces generated for a range of angular diameters. These comparison traces are usually generated assuming a stellar disk with uniform surface brightness. Some investigators generate comparison traces assuming a fully limb-darkened disk ($I = I_0\,\mu$) because this limb function is physically more reasonable for a late-type star with a static atmosphere. It can be shown, however, that the diameter found assuming a fully limb-darkened disk is always $\sim$13% larger than the corresponding diameter found assuming a uniform disk (Ridgway, Wells, and Joyce 1977), so commonly the data are reduced using the uniform brightness disk assumption and then the 13% increase is applied to correct for limb darkening. Other investigators use limb darkening corrections derived from static atmosphere models, but the applicability of static models to Mira variables and other pulsating stars is questionable.

In this study we derived limb functions starting with dynamic models of Mira atmospheres covering a range of phases of the stellar pulsation cycle. Occultation traces were then generated to simulate observations of Mira variables having these limb functions. These traces were compared to traces generated assuming uniform brightness disks with a range of diameters to detemine the diameters that would be derived from standard lunar occultation observations, and these results are compared with the actual diameters of the Mira models used to generate the theoretical Mira occultation traces.

III. THE DYNAMIC ATMOSPHERE MODELS

The dynamic atmosphere models used here were generated by Bowen (1988) and are similar to the model presented by Bowen and Beach (1987) but incorporate improved modeling of cooling for high-temperature regions of the atmosphere.

The model atmospheres are made up of 390 spherical shells

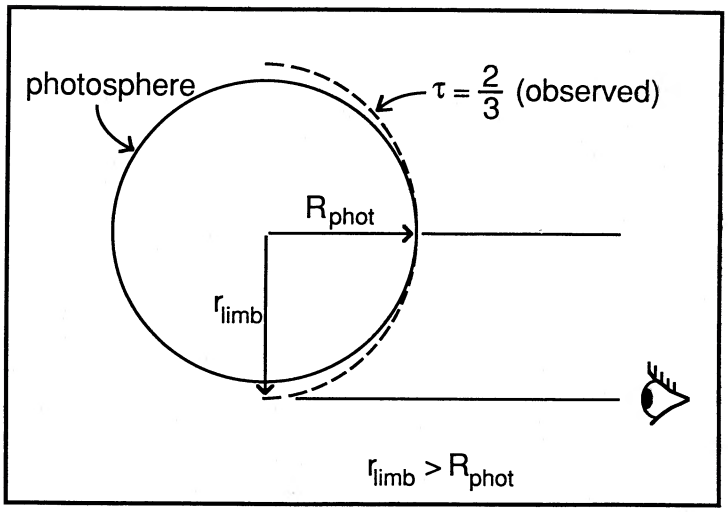

FIG. 1.—Schematic diagram showing apparent size increase due to an extended atmosphere. The radius of the photosphere (R_{phot}) is defined as the radius for which $\tau = \int \kappa\rho\, dx = \frac{2}{3}$, where the integration is along a line of sight through the center of the star. The dotted line indicates where $\tau = \frac{2}{3}$ as seen by an observer. The limb of the star will appear along the line of sight with impact parameter r_{limb}.

to which fundamental hydrodynamic and thermodynamic relations are applied and numerically integrated. The radiative equilibrium temperature in each zone is determined by the Eddington approximation for a spherical gray atmosphere. The rate of thermal relaxation toward the local equilibrium temperature is determined by an empirical function of the local density and temperature. The code includes the effects of radiation pressure on dust which is assumed to form below a condensation temperature of 1500 K. The model atmosphere is driven by sinusoidal variation of the radial position of the innermost boundary, which is typically 10 zones beneath the photosphere. Driving phase 0.0 is defined to occur when the driving boundary is passing through its average radial position, moving outward.

The parameters of the model used in this study are presented in Table 1. The mass, period, and temperature of the model were chosen first; the radius is then determined assuming fundamental-mode pulsation using the period-mass-radius relation of Ostlie and Cox (1986). The decision to use fundamental-mode instead of overtone-mode pulsation is discussed at the end of this section.

The properties of the resulting model at driving phase 0 are presented in Figures 2–4. During each cycle a shock forms and moves outward through the atmosphere. The amplitude of the shock typically reaches a maximum of 35 km s^{-1} and decreases as the shock continues outward. These shocks enormously extend the atmosphere and thereby facilitate dust formation and mass loss.

TABLE 1

MODEL PARAMETERS, MIRA-TYPE VARIABLE

Parameter	Value
Mass	1.2 $M_\odot$
Luminosity	4500 $L_\odot$
T_{eff}	3000 K
Driving period (fundamental mode)	300 days
Driving amplitude	3 km s^{-1}
Photospheric radius (at driving phase 0.0)	1.7321×10^{13} cm
Photospheric radius (static)	1.729×10^{13} cm

The passage of the shock compresses and heats the gas which then radiates away energy as it cools back toward the local equilibrium temperature. The luminosity from the postshock region has a great effect on the limb function of the star. The luminosity history of the inner shock region is presented in Figure 5 which shows the postshock radiated power versus the driving phase for the model atmosphere used here. The "main" shock which forms at driving phase 0.85 is the shock front that moves outward through the atmosphere. The main shock typically forms about 10 zones above the photosphere. A strong shock also forms in the model near driving phase 0.5 when infalling material compresses the region near the piston; the piston at this time has reached its maximum inward velocity and is beginning to slow down. This "preliminary" shock stays at nearly constant radius until the main shock overruns it near driving phase 1.0. The quantitative characteristics of this shock, and possibly its existence, may be determined by the choice of a sinusoidal function to describe the piston motion. The presence of such a shock may be responsible for the "bump" that occurs in the light curves of many Mira variables as the curve rises toward maximum. The morphology of the shock structure in the lower atmosphere also depends on the driving amplitude; At a driving amplitude of 5 km s^{-1} the preliminary and main shocks blend together near phase 0.85 with no discontinuity in luminosity.

The driving phases chosen for the calculation of limb functions were selected on the basis of including a variety of shock structures. Phases dominated by the preliminary strong shock are included since a main shock of this strength would probably result from a more realistic driving function and does occur if a larger driving amplitude is chosen.

The correspondence between the driving phase of the model atmosphere and the phase of the light curve that such a star would display is not known precisely. The phase relationship is a function of the driving amplitude of the model and may need to be determined for each star on a case by case basis. A promising method of determining the phase correspondence involves matching *IUE* observations of Mg II emission from a Mira variable to the luminosity behind the outward moving shocks in the models, as discussed in Brugel, Willson, and Cadmus (1986) and Brugel *et al.* (1988). Based on the analysis

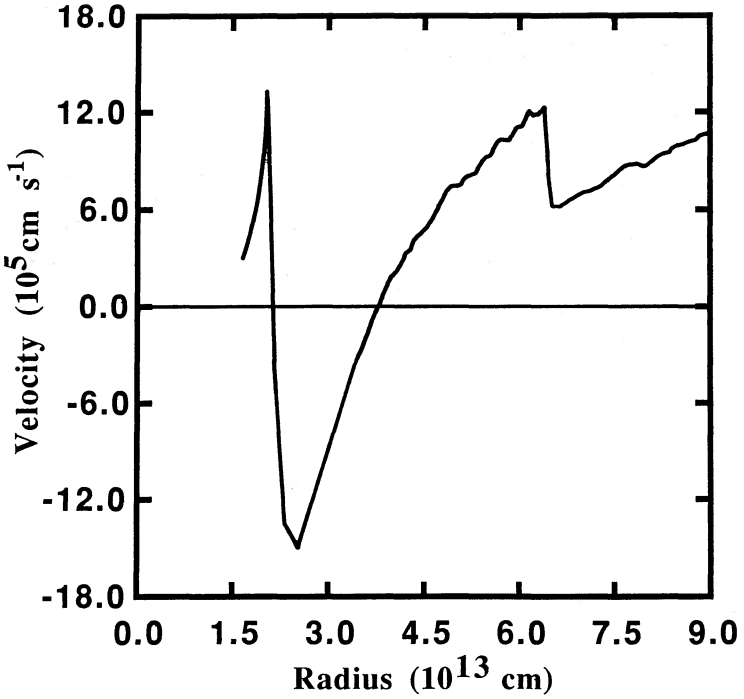

FIG. 2.—Velocity vs. radius for the model atmosphere at phase 0.0. The outward-moving main shock is on the left, and the shock from the previous cycle is on the right.

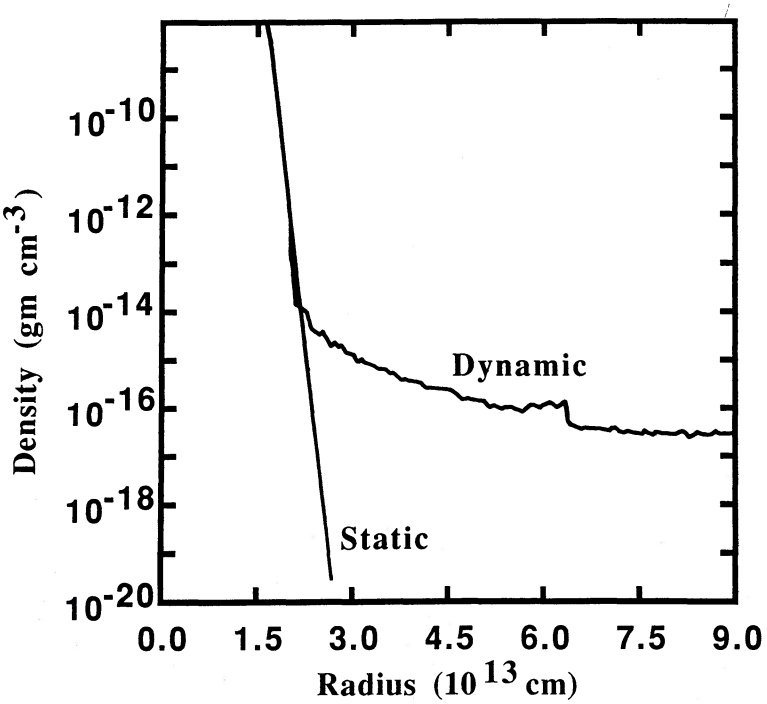

FIG. 3.—Density vs. radius for the model atmosphere at phase 0.0. The static atmosphere case (no driving) is plotted for comparison.

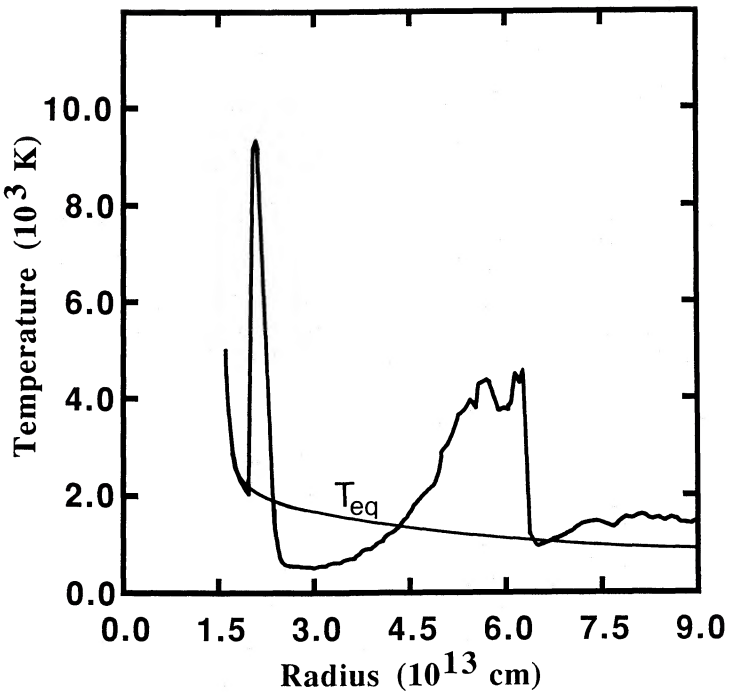

FIG. 4.—Temperature vs. radius for the model atmosphere at phase 0.0. The radiative equilibrium temperature (T_{eq}) vs. radius is also shown.

of data from R Car and T Cep we conclude that phase 0.0 of the light curve coincidentally occurs near driving phase 0.0 of the model.

Model Mira-type atmospheres were also calculated assuming a first-overtone pulsation mode. In order to match the period, luminosity, and mass of the fundamental-mode model, the overtone model requires a radius of 2.705×10^{13} cm ($1.56R_{\text{fundamental}}$) and a temperature of 2400 K. The overtone model must be driven at 1.5 km s^{-1} to produce the same postshock luminosity as the fundamental model driven at 3 km s^{-1}. The densities found in the resulting overtone model atmosphere are approximately 3 orders of magnitude greater than those found in the fundamental-mode model. The optical depth of the dust which forms in the overtone model approaches unity, making it a poor representation of an optical Mira-type star with a 300 day period. The apparent diameter enhancement effects discussed in this paper would be greater for overtone models due to the increased densities. The results presented here, which are based on fundamental-mode models, can be considered as lower bounds in this regard.

IV. THEORETICAL LIMB FUNCTIONS

Limb functions were calculated from the model atmospheres covering a range of driving phases and for two spectral

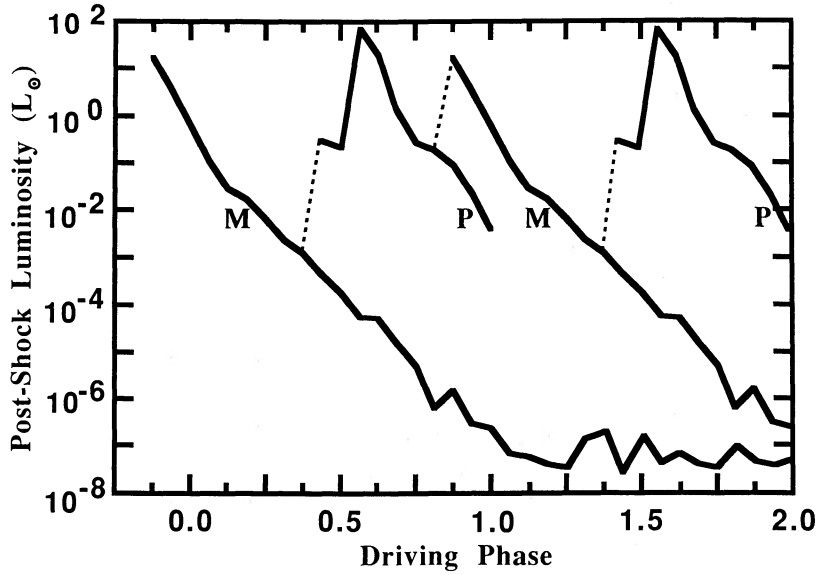

FIG. 5.—Postshock radiated power vs. driving phase for the model atmosphere. The main shocks are labeled "M" and the preliminary shocks are labeled "P." The total power radiated vs. driving phase is approximated well by the value for the strongest shock at each phase, as connected by the dashed lines.

responses. The two bands used were the V band ($\lambda_0 = 550$ nm, $\Delta\lambda = 90$ nm) and the H′ band ($\lambda_0 = 1.618$ μm, $\Delta\lambda = 0.042$ μm). The V band was chosen as representative of an area of the spectrum where postshock cooling radiation dominates (for much of the cycle) over radiation from the stellar photosphere. The H′ band is located at an opacity minimum in the infrared and was chosen as representative of photospheric emission. This opacity minimum is also the reason for the large number of occultation measurements that have been made in this band (Ridgway *et al.* 1982).

The limb functions were calculated for both bands assuming a constant opacity $\kappa = \kappa_R = 10^{-3}$ cm^2 g^{-1} where the subscript R is for Rosseland. This value was used for the gray model atmosphere calculations as it is a fair approximation for the regions of a Mira atmosphere which contribute most to the optical depth (Alexander, Johnson, and Rypma 1983). Another set of limb functions was calculated for the V band assuming a constant opacity of $\kappa = 5\kappa_R$ to simulate observations in a spectral region with enhanced opacity. In all cases a blackbody source function was assumed.

The limb functions were calculated by integrating the intensity inward along lines of sight through the model atmosphere. Assuming a blackbody source function B_ν, a gray atmosphere, and observing in a band characterized by a normalized spectral response, R_ν, the intensity received from the ith segment along the line of sight is given by

$$\Delta I_i = \left\{\left[\kappa_{\rm gas}\int B_\nu(T_{\rm gas})R_\nu\,d\nu\right] + \left[\kappa_{\rm dust}\int B_\nu(T_{\rm dust})R_\nu\,d\nu\right]\right\} \times \kappa_{\rm total}^{-1}[1 - \exp(-\Delta\tau)]\exp(-\tau)\,,$$

where $\kappa_{\rm gas}$ and $\kappa_{\rm dust}$ are the opacities of the gas and dust, respectively, in the ith segment; $\Delta\tau = \rho\,\Delta x\kappa_{\rm total}$ is the change in optical depth across ith segment; and τ is the optical depth between the ith segment and the observer.

The total intensity (integrated over frequency) along the line of sight, is $I = \Sigma_i\,\Delta I_i$. The intensities were calculated for lines of sight with impact parameters out to $1.38R_{\rm phot}$ to include the effects of shocks in the lower atmosphere.

Note that the contribution to the source function of radiation scattered from dust is not considered in this blackbody approximation. In the Mira model used here dust forms near a radius of $2R_{\rm phot}$. The peak intensity of radiation scattered by dust would be expected to occur in an annular region at an impact parameter of $\sim 2R_{\rm phot}$, placing it beyond the range of the limb functions calculated here. The absorption opacity and blackbody radiation of the dust are included because these effects contribute to the integration along the lines of sight which pass through all the layers of the atmosphere. The implications of not including radiation scattered by dust are considered in § V.

The calculated limb functions for the V and H′ bands using $\kappa = \kappa_R$ are presented in Figures 6*a*–6*d*, and for the V band using $\kappa = 5\kappa_R$ in Figures 7*a*–7*d*. The plots show the intensity, integrated over frequency and divided by the central value, plotted versus the impact parameter of the line of sight. A vertical line indicates the position of the $\tau = \frac{2}{3}$ photosphere (as found by integrating $\kappa_R\,\rho\,dx$ inward at an impact parameter of zero) for the current phase. The impact parameters are in units of the photosphere radius at driving phase 0.0.

At phase 0.00 the main shock, which forms above the photosphere, is seen beyond the limb of the star. Phase 0.437 exhibits no shock since the main shock, which has grown considerably weaker, is now beyond the range of radii over which the limb functions were calculated. Phase 0.688 shows the strong, sharp preliminary shock close to the photosphere. At phase 0.815 the preliminary shock has become stalled in the infalling material and is broad and weaker.

The assumption of a blackbody source function may be sufficient for the denser photospheric layers, but it is clearly not valid for the postshock cooling radiation, which is primarily in the form of line emission. The situation may not be all that bad, however, due to a similarity of behavior between the limb functions of the model and an actual Mira-type star. The H′ band limb functions of the models used here are dominated by radiation from the cool photosphere; the hot blackbody postshock region of the model radiates comparatively little in the infrared and therefore the shocks have little effect in the H′ band. The V band limb functions of the model can be dominated by the radiation of the postshock region if a strong shock is present. The blackbody radiation from the hot (typically 6000–10,000 K) postshock region peaks near the visual, whereas, the blackbody radiation from the cool photosphere peaks in the IR and contributes little to the visual. This is particularly true for the enhanced opacity case because the shock contribution is increased while the contribution of the photosphere is now coming from a higher, and therefore cooler, layer and has a smaller fraction of its radiation in the V band. In the case of an actual Mira-type star, the results are qualitatively the same. The H′ band limb functions are dominated by photospheric emission, with little contribution coming from the postshock regions, which are primarily emitting and scattering cooling line radiation. The visual light curve of a real Mira-type star is dominated by the cooling radiation emitted and scattered from the postshock region.

V. SYNTHESIZED DIAMETER MEASUREMENTS

The limb functions were used to generate the Fresnel patterns that would be observed if Mira variables with these limb functions were occulted by the Moon. These theoretical occultation traces were compared to traces that would be produced by uniform surface brightness disks with a range of diameters. The uniform disk trace which "best fits" the Mira trace determines the angular diameter that would be assigned to the Mira variable from lunar occultation observations. To determine the best fit, the squares of the differences between the two traces for all calculated "data" points along the traces were summed, the smallest result representing the best fit. This procedure is considerably simpler than matching uniform disk models to actual observational data because in our case the zero point and the vertical and horizontal scale factors are known.

The occultation traces for the uniform surface brightness reference models were generated as outlined by Nather and McCants (1970). The stellar disk is divided into a series of equal-width strips parallel to the limb of the Moon. Each strip is replaced by a point source whose intensity is equivalent to the total brightness of the strip (the total brightness is proportional to the area of the strip for the uniform brightness case). The Fresnel patterns of all the point sources are shifted relative to each other due to their different angular separations from the limb of the Moon. These overlapping, shifted patterns add together and form the occultation trace observed at the surface of the Earth. The occultation traces for the Mira models having the theoretical limb functions were generated in the same manner except that the brightness of the ith strip is

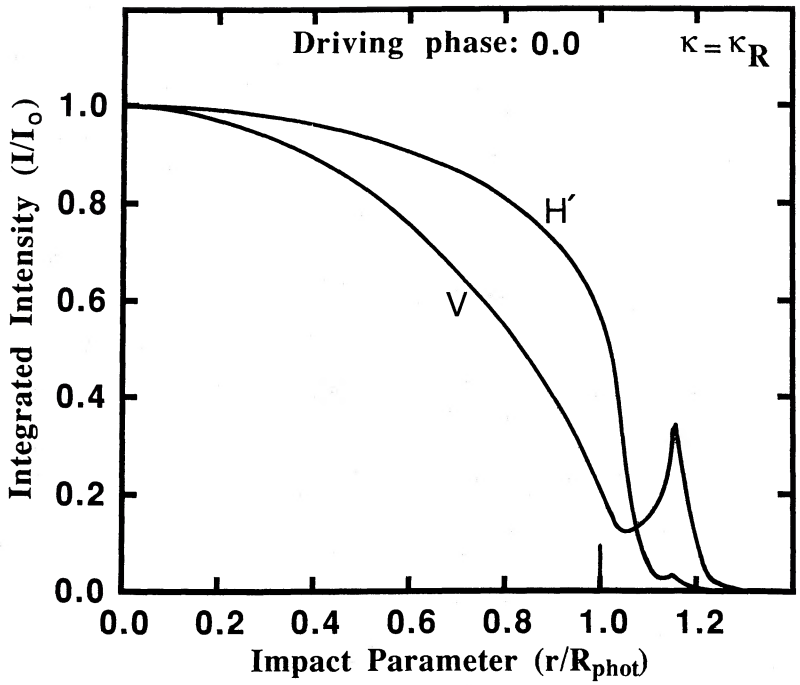

FIG. 6*a*

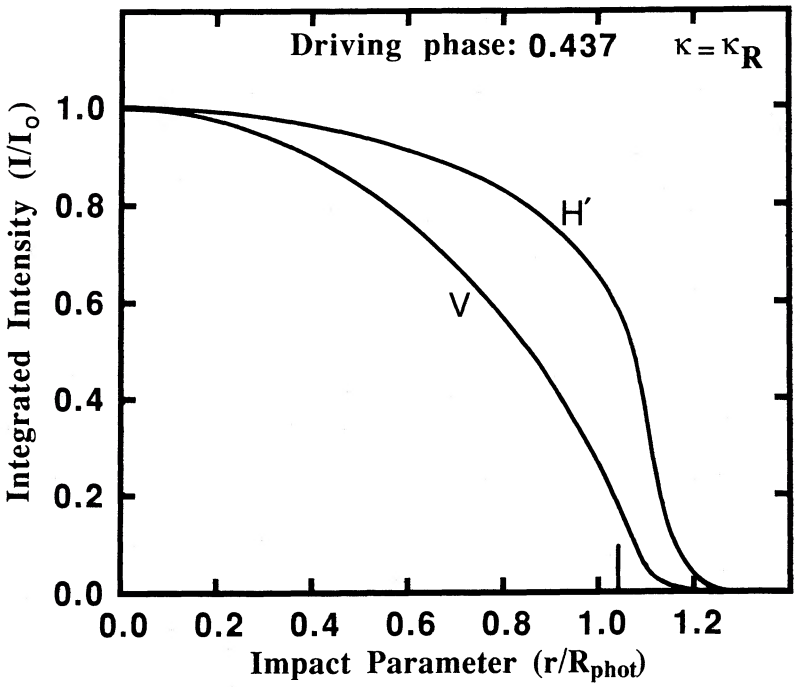

FIG. 6*b*

FIG. 6.—Model limb functions for the H′ and *V* bands, assuming $\kappa = \kappa_R$, at driving phases 0.0 (*a*), 0.437 (*b*), 0.688 (*c*), and 0.815 (*d*).

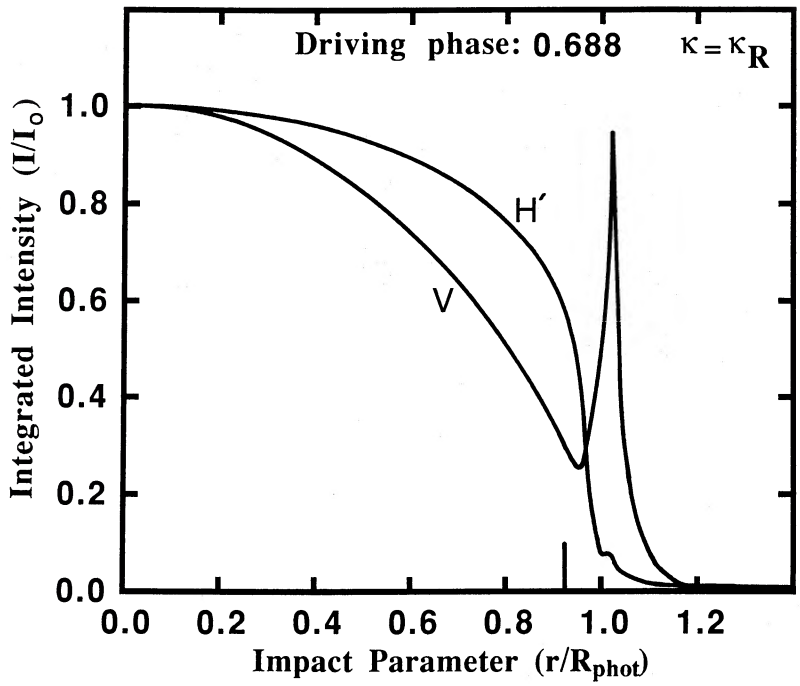

FIG. 6c

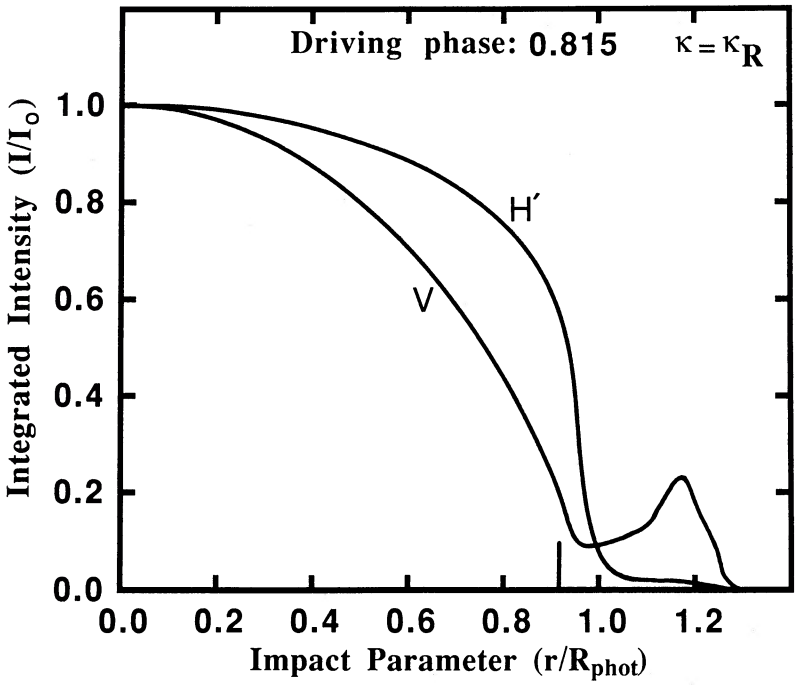

FIG. 6d

now $b_i = \int_{\text{strip}} I(r)dA$, where $I(r)$ is the limb function and r is the impact parameter.

Occultation traces were calculated for the model Mira variables using two different size scales, one with geometrical angular diameter (at driving phase 0.0) of 0".0047, and the other with angular diameter of 0".026. When comparing the Mira traces to the best-fitting uniform disk traces, it was found that the relative diameters were independent of the angular diameter scale used over this range. Our results are therefore given in units of the geometrical diameter of the $\tau = \frac{2}{3}$ photosphere at driving phase 0.

Typical generated occultation traces are shown in Figures 8–10. Figure 8 shows the occultation trace in the V band for the 0".0047 angular diameter Mira variable at phase 0.0 generated assuming the $\kappa = \kappa_R$ limb function. The best-fitting uniform disk trace is also plotted, offset vertically for clarity.

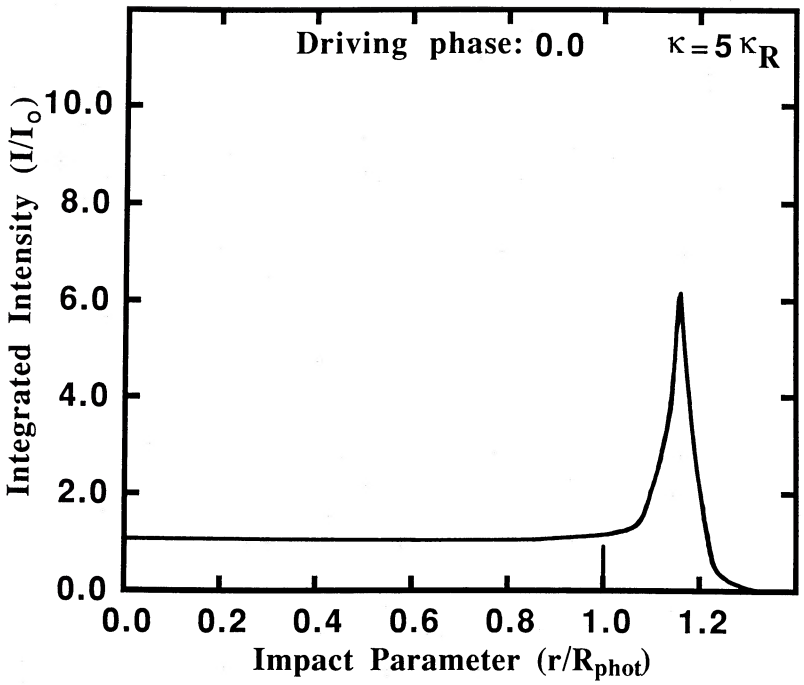

FIG. 7*a*

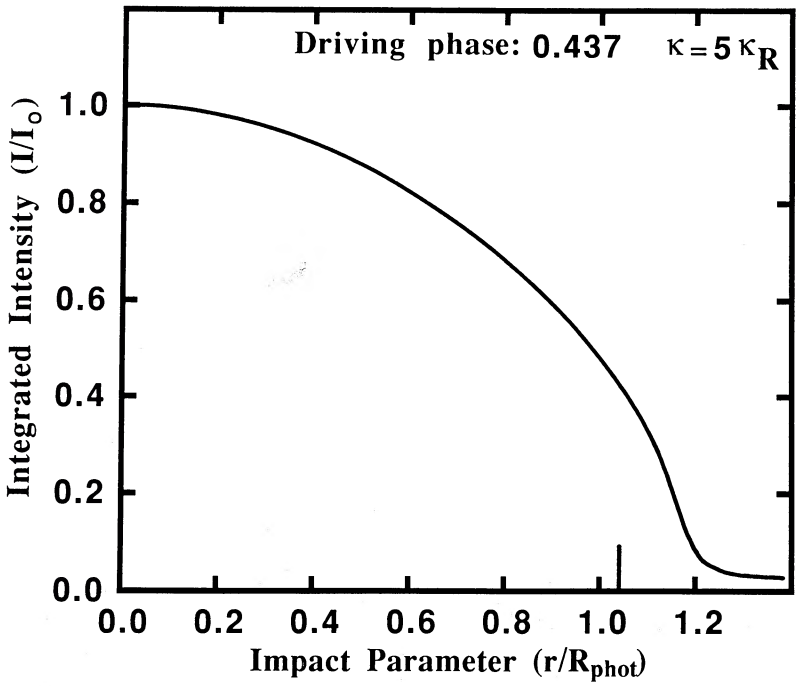

FIG. 7*b*

FIG. 7.—Model limb functions for the *V* band, assuming $\kappa = 5\kappa_R$, at driving phases 0.0 (*a*), 0.437 (*b*), 0.688 (*c*), and 0.815 (*d*).

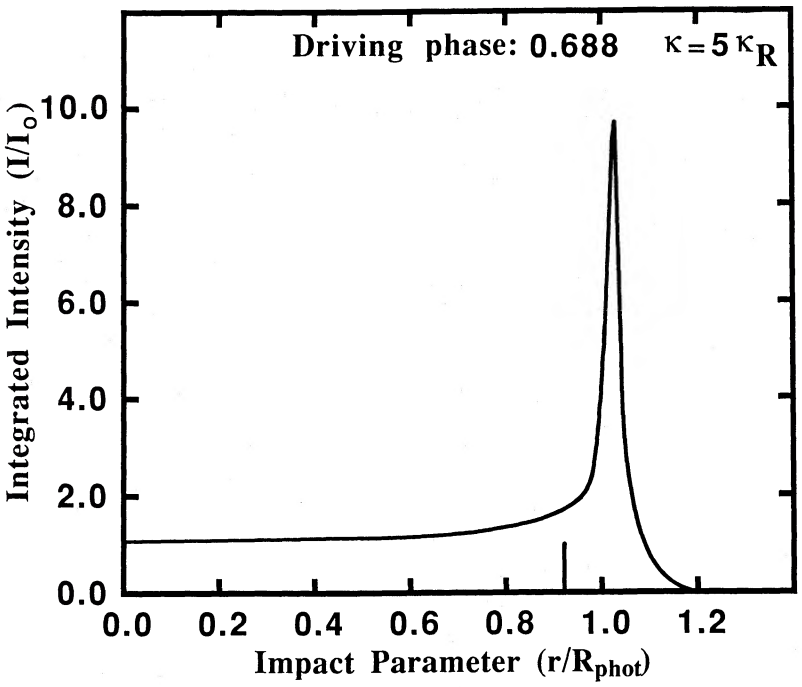

FIG. 7c

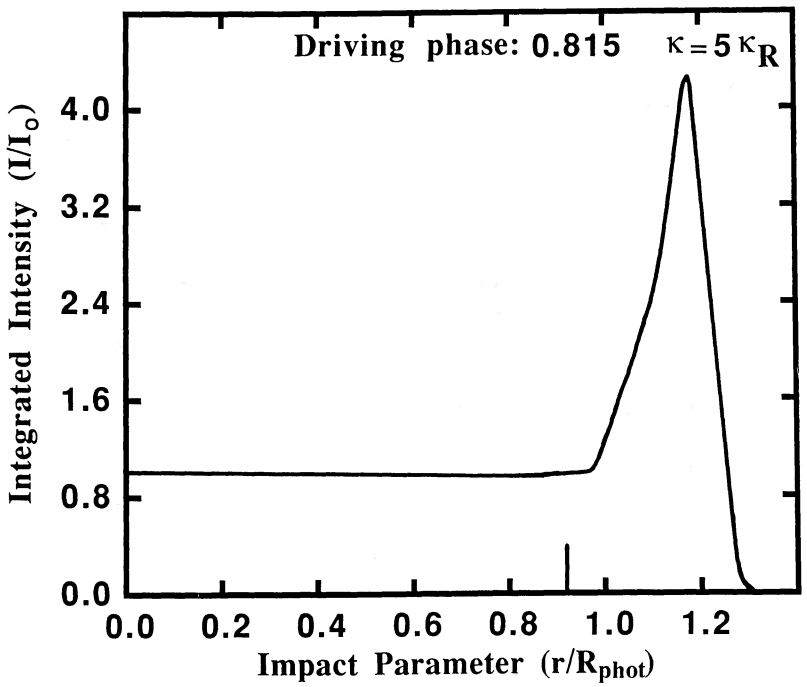

FIG. 7d

Figure 9 shows similar traces for the 0.″026 angular diameter Mira variable at phase 0.0 using the $\kappa = \kappa_R$ limb function. Also shown in Figure 9 is the best-fitting trace from a fully limb-darkened disk. The presence of the shock in the limb function does not cause the occultation trace of the Mira variable to appear noticeably unusual in shape compared to the fully limb-darkened trace.

A case with a more extreme shock is displayed in Figure 10, which shows the occultation trace in the V band for a 0.″024 angular diameter Mira variable at phase 0.688 using the $\kappa = 5\kappa_R$ limb function which is dominated by powerful shock emission. The best-fitting uniform disk and fully darkened disk traces are also presented for comparison. In this extreme case the occultation trace shows characteristics of this "bright ring" limb function, but the effect is not as great as might be expected considering the dominance of the limb function by the shock emission.

As a check of the program used, an occultation trace was

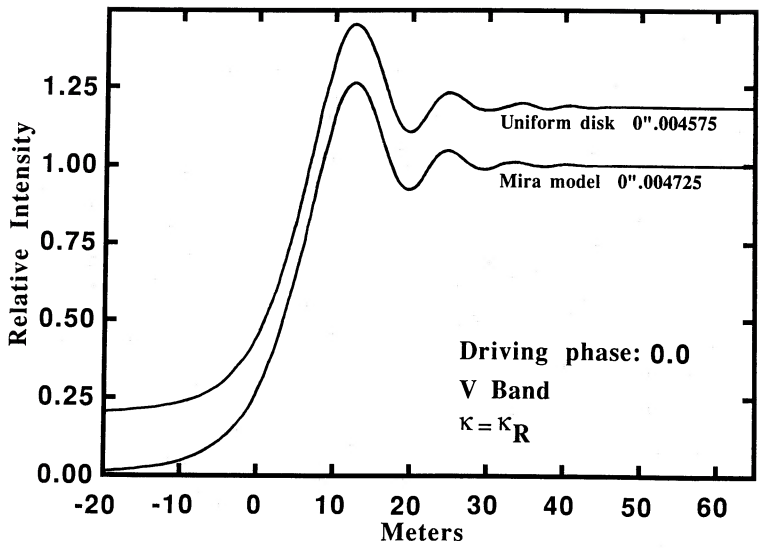

FIG. 8.—Theoretical V band occultation trace for a Mira-type model with angular diameter of 0".004725, using the limb function for driving phase 0.0 and $\kappa = \kappa_R$. The best-fitting uniform disk trace, from a uniform disk with diameter 0".004575, is plotted offset vertically for comparison.

prepared for a fully limb-darkened disk and compared to the uniform disk traces. The fully limb-darkened disk was found to be 13.2% larger than the best-fitting uniform brightness disk, as expected.

The results of fitting uniform disks to the model Mira variables are presented in Tables 2–4. The geometrical angular diameter of the gray atmosphere photosphere at each phase is labeled Φ_{phot}. These values are given in units of the angular diameter at phase 0.0. The photosphere diameter at each phase is constant for all bands and opacities since it represents the

TABLE 2

ANGULAR DIAMETERS: H′ BAND, $\kappa = \kappa_R$

Driving Phase	Φ_{phot}	Φ_{UD}	Error–UD	Φ_{FLD}	Error–FLD
0.000.....	1.000	1.000	0.0%	1.132	+13.2%
0.252.....	1.094	1.104	+1.0%	1.250	+14.3%
0.437.....	1.042	1.058	+1.5%	1.198	+15.0%
0.688.....	0.923	0.931	+1.0%	1.054	+14.2%
0.815.....	0.919	0.923	+0.5%	1.045	+13.7%

TABLE 3

ANGULAR DIAMETERS: V BAND, $\kappa = \kappa_R$

Driving Phase	Φ_{phot}	Φ_{UD}	Error–UD	Φ_{FLD}	Error–FLD
0.000.....	1.000	0.965	−3.5%	1.092	+9.2%
0.252.....	1.094	0.965	−12.0%	1.092	−0.3%
0.437.....	1.042	0.919	−12.0%	1.040	−0.2%
0.688.....	0.923	0.956	+3.5%	1.082	+17.2%
0.815.....	0.919	0.927	+1.0%	1.049	+14.1%

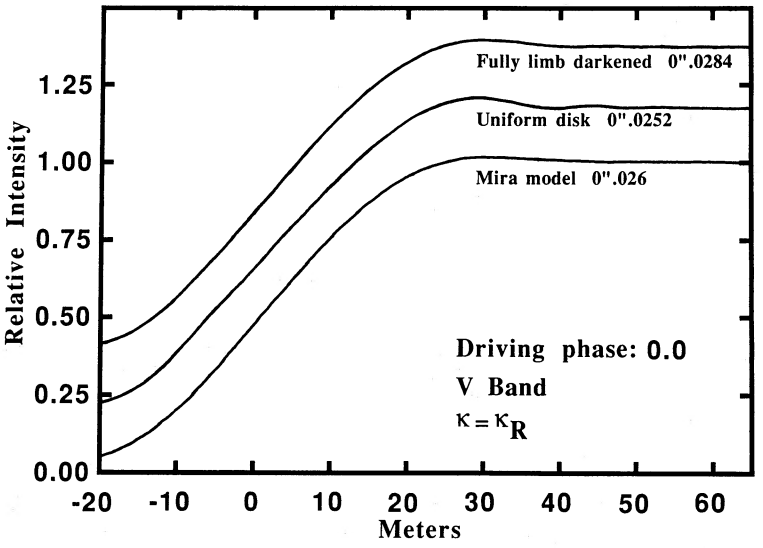

FIG. 9.—Theoretical V band occultation trace for a Mira-type model with angular diameter of 0".026, using the limb function for driving phase 0.0 and $\kappa = \kappa_R$. The best-fitting uniform disk trace (disk diameter = 0".0252) and the best-fitting fully limb-darkened disk trace (disk diameter = 0".0284) are plotted offset vertically for comparison.

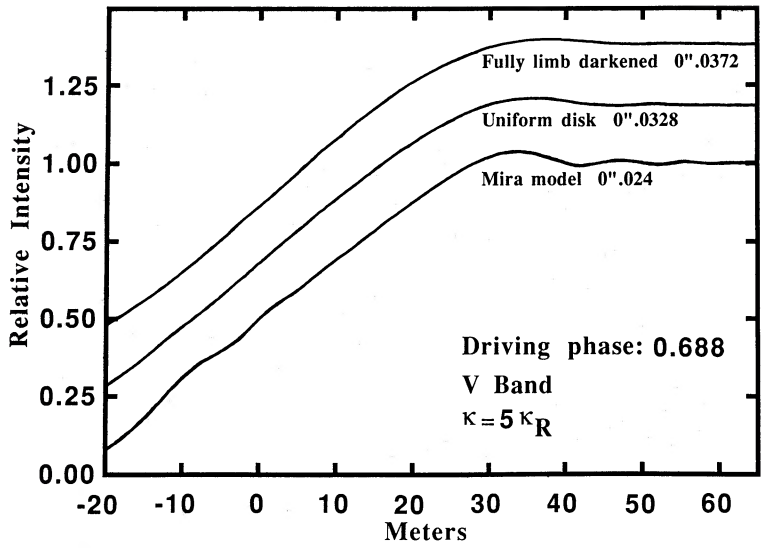

FIG. 10.—Theoretical V band occultation trace for a Mira-type model with angular diameter of 0.″024, using the limb function for driving phase 0.688 and $\kappa = 5\kappa_R$. The best-fitting uniform disk trace (disk diameter = 0.″0252) and the best-fitting fully limb-darkened disk trace (disk diameter = 0.″0284) are plotted offset vertically for comparison. Variations in the model Mira trace due to the extreme shock-induced limb brightening are apparent.

diameter of the Mira variable at the (constant) Rosseland mean opacity. The angular diameter of the best-fitting uniform brightness disk is labeled Φ_{UD}, specified in the same units. The value labeled "error–UD" indicates the percent difference between Φ_{UD} and the true angular diameter of the Mira variable given by Φ_{phot}. A positive value for error–UD means Φ_{UD} overestimates the true angular diameter, while a negative value means Φ_{UD} underestimates the true angular diameter. The fully limb-darkened angular diameter Φ_{FLD} is obtained by multiplying Φ_{UD} by 13.2% (representing an extreme correction for limb darkening). The value labeled error–FLD indicates the percentage difference between Φ_{FLD} and the true geometrical angular diameter.

As can be seen from the tables, the "correction" for limb darkening is not always desirable, and in some cases it represents a change in the wrong direction. In the H′ band, Φ_{UD} provides a good measure of the actual model diameter, and Φ_{FLD} overestimates the diameter. Corrections derived from static models, although less severe than the full limb-darkening correction, will also result in an overestimate of the true diameter.

The V band is somewhat more complicated. When no strong shock is present (near minimum light), Φ_{FLD} gives a good estimate of the true diameter. When a shock is present, the proper limb-darkening correction required depends on the strength and position of the shock and must be obtained from dynamic atmosphere models.

The situation is even more complex in the enhanced opacity V band case where the (mild) opacity enhancement accentuates the effect of the shocks. When a shock is present, the limb function resembles a bright ring (surrounding a dim disk), and the diameters obtained by comparison to uniform brightness disks are not very meaningful. It would be useful to make observations (using either speckle interferometry or occultation) in a narrow band centered on the hydrogen Balmer emission lines. Analyzing these observations using ring-dominated limb functions would allow the angular diameter of the shock front to be measured.

Including radiation scattering by dust would surround the stellar image with a diffuse annular region at an impact parameter of $\sim 2R_{phot}$. An angular diameter derived without considering the contribution of this region would overestimate the true angular diameter. However, it seems likely that the dust annulus would be ignored by the data analysis procedure used for occultation measurements because the Fresnel pattern of the annulus would be characteristic of a diameter about twice that of the photosphere. The uniform disk model trace which best fits the occultation trace would be characteristic of the much stronger photosphere pattern; increasing Φ_{UD} slightly would improve the fit to the Fresnel pattern of the dust annulus, but it would much more rapidly degrade the fit to the stronger Fresnel pattern of the photosphere.

TABLE 4

ANGULAR DIAMETERS: V BAND, $\kappa = 5\kappa_R$

Driving Phase	Φ_{phot}	Φ_{UD}	Error–UD	Φ_{FLD}	Error–FLD
0.000.....	1.000	1.404	+40.5%	1.589	+58.9%
0.252.....	1.094	1.110	+1.5%	1.256	+14.8%
0.437.....	1.042	1.046	+0.5%	1.184	+13.6%
0.688.....	0.923	1.262	+36.5%	1.429	+54.8%
0.815.....	0.919	1.442	+57.0%	1.632	+77.6%

VI. CONCLUSIONS

Dynamic effects in the atmospheres of Mira-type variables cause these stars to appear larger (and therefore cooler) than they actually are. Standard methods for measuring stellar angular diameters require the assumption of a limb function, but the limb functions derived from static atmosphere models are not valid for Mira variables (and probably not for semiregular variables, either). Stellar pulsations cause atmospheric shocks which affect the limb function of a Mira variable by extending the atmosphere and by the emission of substantial postshock cooling radiation.

The limb-function correction required to derive Φ_{true} from Φ_{UD} is a function of the wavelength of observation and the phase of the pulsation cycle. Specifically, for observations in the H′ band, $\Phi_{true} \approx \Phi_{UD}$ (no correction for limb darkening

should be applied). For observations in the V band, or any other band where shock luminosity is significant, the limb-function correction (Φ_{true}/Φ_{UD}) depends on the shock strength and position and therefore varies greatly with phase.

We recommend that observers should always publish Φ_{UD} values. Investigators should apply limb-function corrections with care, conscious of the need to use limb functions derived from dynamic models. Our results can serve as a guide, but refined modeling is needed, including improved dynamic model atmospheres, modeling of postshock emission, and better handling of radiative transfer.

REFERENCES

Alexander, D. R., Johnson, H. R., and Rypma, R. L. 1983, *Ap. J.*, **272**, 773.
Bowen, G. H. 1988, *Ap. J.*, **329**, 299.
Bowen, G. H., and Beach, T. E. 1987, in *Late Stages of Stellar Evolution* (Calgary, Alberta, Canada), ed. S. Kwok and S. R. Pottasch (Dordrecht: Reidel), p. 275.
Brugel, E. W., Beach, T. E., Willson, L. A., and Bowen, G. H. 1988 in *IAU Colloquium 103, The Symbiotic Phenomenon*, ed. M. Friedjung (Dordrecht: Reidel) in press.
Brugel, E. W., Willson, L. A., and Cadmus, R. 1986, in *New Insights in Astrophysics, Eight Years of Astronomy with IUE* (ESA SP-263), p. 213.
Labeyrie, A., Koechlin, D., Bonneau, D., Blazit, A., and Foy, R. 1977, *Ap. J. (Letters)*, **218**, L75.
Nather, R. E., and McCants, M. M. 1970, *A.J.*, **75**, 963.
Ostlie, D. A., and Cox, A. N. 1986, *Ap. J.*, **311**, 864.
Ridgway, S. T., Jacoby, G. H., Joyce, R. R., Siegel, M. J., and Wells, D. C. 1982, *A.J.*, **87**, 808.
Ridgway, S. T., Joyce, R. R., White, N. M., and Wing, R. F. 1980, *Ap. J.*, **235**, 126.
Ridgway, S. T., Wells, D. C., and Joyce, R. R. 1977, *A.J.*, **82**, 414.
Willson, L. A. 1982, in *Pulsations in Classical and Cataclysmic Variable Stars*, ed. J. P. Cox and C. J. Hansen (Boulder: JILA), p. 269.

THOMAS E. BEACH, GEORGE H. BOWEN, and LEE ANNE WILLSON: Astronomy Program, Department of Physics, Iowa State University, Ames, IA 50011